Proceedings of the ASME 2022
International Mechanical Engineering Congress and Exposition
IMECE2022
October 30-November 3, 2022, Columbus, OH, USA

IMECE2022-95243

MULTISCALE MODELING OF THE UPTAKE OF HYDROGEN CHLORIDE ON ANODIZED ALUMINUM IN RELEVANCE TO SPACECRAFT FIRE SAFETY

Justin Niehaus[1,2], Sandip Mazumder[2]

[1]NASA Glenn Research Center, Cleveland, Ohio, 44135, USA
[2]Department of Mechanical and Aerospace Engineering, The Ohio State University, Columbus, OH 43210, USA

ABSTRACT

Fire safety is a critical component of space missions. An electrical fire within the spacecraft often produces gaseous hydrogen chloride (HCl) from the smoldering of wire insulation. These gases tend to stick to the interior materials of the spacecraft, which is often comprised of treated aluminum. Determining the rate of uptake for HCl by aluminum helps the safe design of the spacecraft to reduce catastrophic mission risk. Our previous studies showed that a one-step global reaction model for adsorption of HCl on aluminum is incapable of predicting the experimentally measured HCl uptake of anodized aluminum, compared to other treatments with thinner oxide layers. X-ray photoelectron spectroscopy revealed that aluminum chloride is found deep in the oxide layer of the anodized aluminum, implying that the transport of HCl within the oxide layer covering the aluminum surface must be considered. This work uses a multiscale modeling approach to predict the uptake of HCl. A pore model is developed wherein the HCl reacts with the aluminum oxide pore walls to create an aluminum chloride layer. The HCl then diffuses through that layer for further reaction, until the diffusion resistance grows too large, and the surface is said to be saturated. The pore model is then coupled with the reactor-scale model to predict overall HCl uptake. Results show that this new multiscale approach predicts the uptake of HCl far more accurately than previously used single-scale models.

Keywords: Spacecraft Fire Safety, Multiscale Modeling, Surface Reactions

NOMENCLATURE

A	Pre-exponential factor, 1/s
A_{po}	Surface area of pore, m^2
c	Concentration, mol/m^3
CCC	Chromate Conversion Coating
D_{eff}	Effective diffusion coefficient, m^2/s
D_{op}	Diffusion coefficient through open pore, m^2/s
D_{pl}	Diffusion coefficient in product layer, m^2/s
E_a	Activation energy, J
PVC	Poly (vinyl chloride)
k	Reaction rate constant for reactor model, 1/s
k_r	Reaction rate in pore model, m/s
M	Molar Mass, kg/mol
MFC	Mass Flow Controller
m_{HCl}	Mass of HCl deposited on pore walls, kg
R	Universal gas constant, J/(mol-K)
$\dot{R}$	Reaction rate for reactor model , $kmol/(m^3\text{-}s)$
s	Surface site used by reactor model
SEM	Scanning electron microscopy
T	Temperature, K
XPS	X-ray photoelectron spectroscopy
ε_{opl}	Volume fraction of product layer
ε_{pl}	Volume fraction of product layer
ρ_{site}	Surface site density
θ	Surface site fraction
μ	Site dependent exponential factor

INTRODUCTION

As missions in space become longer and more complex, fire safety becomes a critical issue. Most fire testing that has been used in spacecraft design takes place in 1-g or at small-scale [1-3]. There are experiments underway to address gaps in knowledge of smoke and flame spread in a large-scale microgravity environment, as well as provide the opportunity to test novel gas species sensor technology and understand the effect the fire has on the vehicle [4-7]. One of these knowledge gaps is the fate of acid gas after a fire.

Risk assessments cite an electrical fire as a common spacecraft scenario [8]. Combustion products from the smoldering of wire insulation include acid gases such as

hydrogen chloride (HCl), hydrogen fluoride (HF) and hydrogen cyanide (HCN). These gases pose a threat to crew health and safety, as well as provide an opportunity for additional fire detection methods. It is important to study the interaction of these gases with surfaces to determine their lifetime within the spacecraft environment for potential fire detection and post-fire cleanup applications, as well as general crew safety. These gases adsorb on surfaces and participate in other reactions, unlike more common combustion products such as water and carbon dioxide. Studies in terrestrial fires show that HCl from pyrolyzed poly(vinyl chloride) (PVC) reached a peak in the atmosphere and then decreased rapidly in rooms made of Poly(methyl methacrylate) (PMMA), painted gypsum, ceiling tile and cement block [9,10].

Aluminum is abundant inside a spacecraft and is often treated to enhance its natural oxide layer, known as alumina [11, 12]. Chromate conversion coating (CCC) creates a thin enough barrier to allow electricity to still be conducted through the metal, while anodization creates a much thicker and protective alumina layer that cannot conduct electricity. Both these treatments are commonly used in spacecrafts.

Previous work has studied the interaction of HCl with treated and untreated aluminum [13,14]. A reactor was built to flow HCl over a cylindrical sample, measuring the inlet and outlet concentration of HCl to determine the rate of uptake. A numerical model of the reactor was developed where a one-step global reaction that accounted for active surface sites was used for modeling HCl uptake. The model reaction rate constants were calibrated to the untreated and CCC aluminum experimental results. When used for anodized aluminum, though, the same model did not match as well with experimental data. The untreated aluminum and the CCC aluminum were inspected using X-Ray Photoelectron Spectroscopy (XPS) and found to have oxide layer thicknesses of 50 and 200 nm respectively, while the anodized aluminum had an oxide layer thickness of 5,500 nm. With an order of magnitude thicker oxide layer, the mass transport resistance of the oxide layer becomes critical and the effect of diffusion through the pores of the oxide layer must be accounted for.

On account of the huge disparity in length scales, it is not feasible to model the diffusion through the pores of the oxide layer within the reactor-scale model. In other words, the same mesh that resolves the inside of the reactor cannot be also used to resolve the pores within the oxide layer covering the aluminum surface. It is with this difficulty in mind, a separate pore-scale model was first developed and used to compute the growth of the aluminum chloride layer and its effect on HCl uptake [15]. This subgrid-scale model assumes the pores to be cylindrical and the reaction of HCl with aluminum oxide pore walls to create aluminum chloride is considered. The HCl then must diffuse through the thickening aluminum chloride layer to react. The reaction stops when the diffusion resistance becomes too large for more HCl to make it to the pore wall. The output of this pore model was ultimately used in the reactor-scale model to result in what is referred to here as a *multiscale* model. This is accomplished by increasing the diffusion resistance realized in the pore model. Using the time dependent decrease in diffusion coefficient, an expression for the diffusion coefficient as a function of HCl wall concentration is further developed to make the expression more general and applicable to other simulation parameters. The overall idea is depicted in Figure 1.

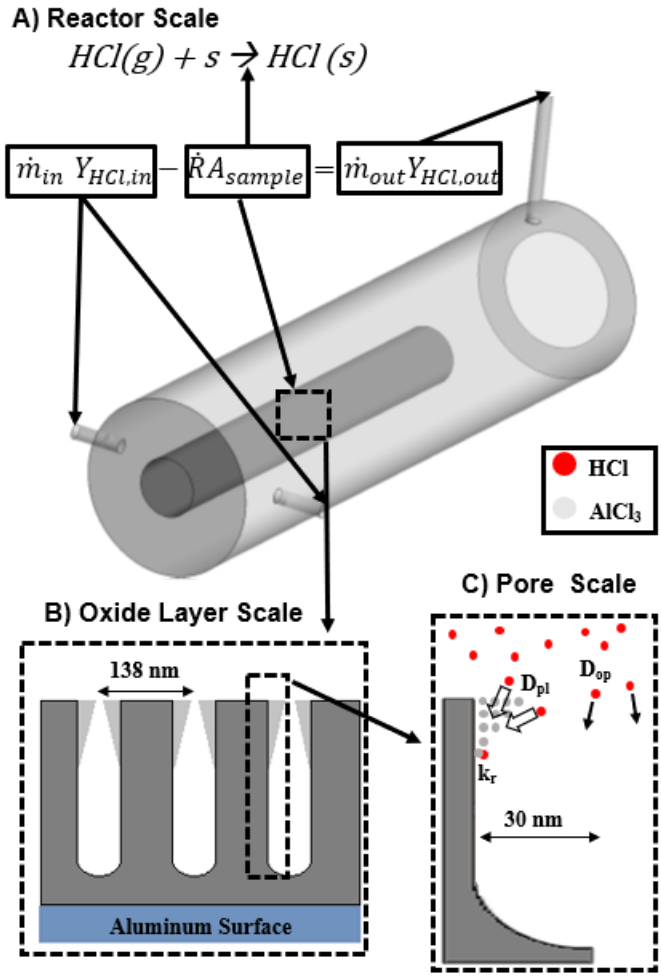

Figure 1: Multiscale model schematic. *A 3D rendering of the reactor model is given by (A), where HCl only reacts with active surface sites. When the sites are filled, the sample is saturated, and the reaction stops. The pore model allows HCl to diffuse into the porous oxide layer (B) and react with the aluminum oxide walls to create an aluminum chloride product layer (C).*

MATERIALS AND METHODS

Experimental Measurements

First, experiments were carried out where HCl flowed into a reactor over an aluminum sample to determine the HCl uptake. These tests were used to calibrate the constants in a one-step global reaction. A schematic of the test reactor is shown in Figure 2. It was constructed out of cast acrylic, as it was not known to react with HCl. Air mixed with approximately 45 parts per

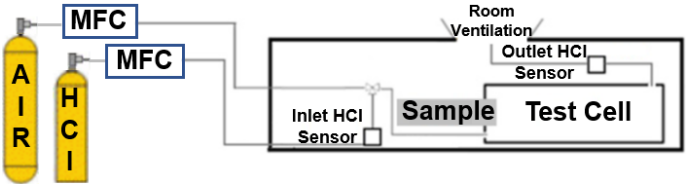

Figure 2: Schematic of laboratory setup. *The sample is pushed into the test cell after inlet and outlet HCl sensors showed equilibrium.*

million (ppm) of HCl is flowed through the test reactor at 1000 cubic centimeters per minute (ccm). Electrochemical HCl sensors with a range of up to 50 ppm and a resolution of 0.1 ppm were placed at the inlet and outlet of the reactor to determine the uptake of the sample. The sample was pushed by air pump into the reactor after the concentration on each sensor had reached steady state. During the test, the inlet concentration remains relatively constant, while the outlet sensor drops, and then increases back up to the initial value as the sample saturates.

Aluminum 6061-T6 were used for the study and were treated by anodizing to standard MIL-8635F Type II Class 1, or by CCC using standard MIL-DTL-5541F Type I. The test samples were 2.54 cm in diameter by 30 cm in length, while at baseline tests push 20 cm of sample length. XPS was used to determine the oxide layer thickness of the aluminum samples, as well as the depth of the chlorine found in the samples after the test. The oxide layer thickness was found to be 50 nm for the untreated aluminum, 200 nm for the CCC and 5,500 nm for the anodized. On average, chlorine was found no lower than 5, 50, and 2,200 nm for the untreated, CCC and anodized aluminum respectively. These values are found in Table 1, along with the site density of each aluminum treatment, which is explained in the next section.

Table 1: Oxide Layer thickness, depth chlorine is found within the oxide layer after a test and site density of aluminum used in the study.

Aluminum Treatment	Depth of Oxide Layer (nm)	Depth Chlorine Found by XPS (nm)	Site Density ($kmol/m^2$)
Untreated	50	5	7.61×10^{-8}
CCC	200	50	4.09×10^{-7}
Anodized	5,500	2,200	2.90×10^{-6}

Reactor Model

Figure 3 shows a schematic of the reactor model, along with associated boundary conditions. It is a 2D axisymmetric model with an annular mass flow inlet, a reacting surface (aluminum surface) with a 1-step global reaction rate, and a pressure outlet. The one-step global reaction that was used is as follows:

$$HCl(g) + s \rightarrow HCl(s) \qquad (1)$$

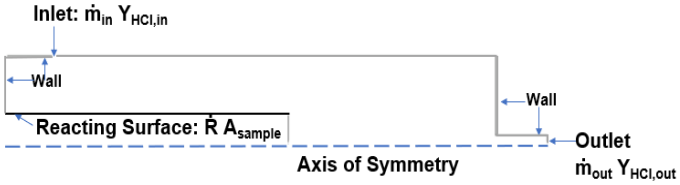

Figure 3: Schematic of reactor model.

HCl(g) represents gaseous HCl, while *s* is an active surface site. *HCl(s)* denotes adsorbed HCl. The rate of HCl disappearance from the reactor equals the rate of aluminum surface site consumption and is given by:

$$\frac{\partial [HCl]}{\partial t} = \frac{\partial [s]}{\partial t} = \dot{R} = k[HCl]^a[s]^b \qquad (2)$$

The quantities in square brackets describe molar concentrations in $kmol/m^3$, while $\dot{R}$ is the molar reaction rate and k is the reaction rate constant. This constant is expressed by an Arrhenius rate expression that accounts for surface coverage:

$$k = A_p T^{\beta} e^{\frac{-E_a}{RT}} \theta^{\mu} e^{\frac{-\varepsilon}{RT}} \qquad (3)$$

The site fraction θ is the ratio of active sites remaining [*s*] and the total site concentration known as the surface site density, ρ_{site}. This site fraction has a starting value of unity, and as the active sites fill up, decreases towards zero. This ultimately brings k from its maximum value, down to zero as the surface saturates. All experiments in this work were conducted at room temperature (20 °C), allowing the temperature dependent terms to be treated as constants, ultimately combined into the calibratable constant *A*. Furthermore, the global reaction stated in Eq. (1) was assumed to be first order in HCl (a = 1) as evidenced in previous studies [16,17]. Consequently, Eq. 3 simplifies to:

$$\dot{R} = A[HCl][s]\theta^{\mu} \qquad (4)$$

Figure 4 shows the experimental results from the three types of aluminum tested. The curves are integrated to determine ρ_{site}, which is used as an input into the model. The available sites correlate positively with the thickness of the oxide layer, as can be seen in Table 1. The constants of the 1-step global reaction were calibrated using the CCC experiment, since it had the intermediate number of sites. Figure 5 gives the calibrated results for the CCC treatment. An A value of 30,000 and μ of 1 was used as the best match, and validated with different flow values, inlet concentrations and sample lengths. More information about the calibration process, as well as mesh independence is given in previous work [13]. The reaction rate calibrated for the CCC fit the untreated aluminum sample as well, which is also demonstrated in Figure 5. The anodized aluminum did not fit as

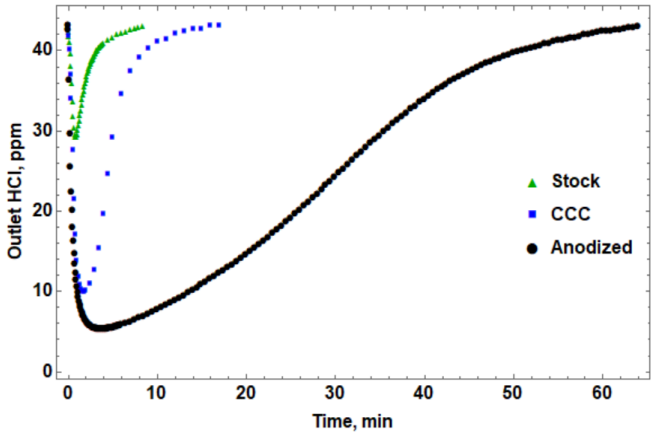

Figure 4: Experimental HCl history at the outlet sensor.

well, as shown in Figure 6. This is likely due to the additional mass transport resistance posed by a thicker oxide layer and is the central focus of the present study. As discussed earlier, a multiscale model that integrates a pore-scale and a reactor-scale model is proposed. In the next subsection, the pore model is discussed.

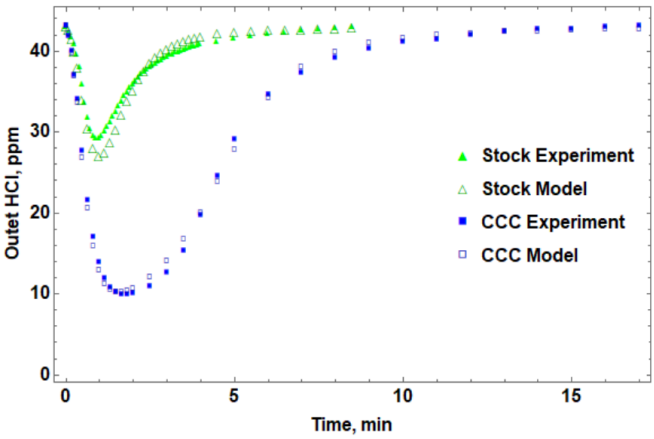

Figure 5: Stock and CCC experiments with calibrated reactor model. *A =30,000 and μ = 1.0.*

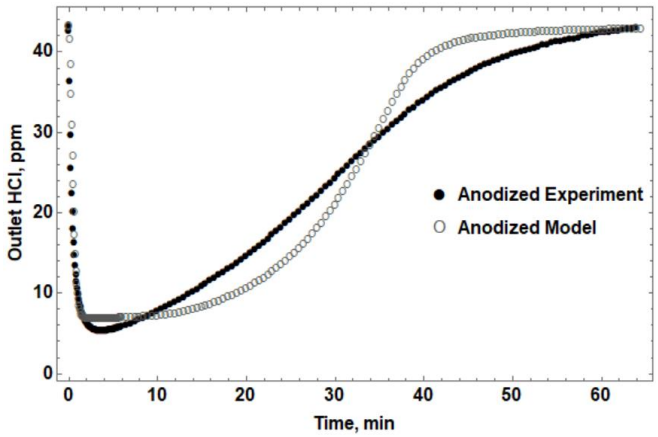

Figure 6: Anodized experiment with calibrated reactor model. *A =30,000 and μ = 1.0.*

Pore Model

To account for the mass transport and reaction (formation of aluminum chloride) within the oxide layer, a pore-scale model was developed for a single pore in the oxide layer. A 2D axisymmetric model of a single cylindrical pore was used for the diffusion of HCl into the pore, with the top boundary condition being of constant concentration and a boundary condition set at the pore walls representing the reaction of HCl with aluminum oxide. In this model, the reaction at the pore wall creates a solid aluminum chloride layer that the HCl must diffuse through to further react (see bottom right subfigure of Fig. 1). Once the layer grows too thick, the sample is said to be saturated and the reaction slows to a stop. HCl transport through the pore is described by the 2D transient diffusion equation given by:

$$\frac{\partial c}{\partial t} = \frac{1}{r}\frac{\partial}{\partial r}\left(rD\frac{\partial c}{\partial r}\right) + \frac{\partial}{\partial z}\left(D\frac{\partial c}{\partial z}\right) \qquad (5)$$

The concentration of HCl in mol/m^3 is denoted by c while the diffusion coefficient in m^2/s is denoted by D. The concentration of HCl at every control volume (cell) center is determined by discretizing Eq. (5) using the finite volume method [18]. Time advancement is implemented using the implicit backward Euler method. When HCl reaches the pore wall, it creates a solid aluminum chloride and deposits on the pore wall at the rate given by:

$$m_{HCl} = k_r\, c_w\, A_{po}\, M\, dt \qquad (6)$$

The reaction rate, HCl wall concentration and area of the pore are given by k_r, c_w, and A_{po}, respectively. The molar mass of the product (aluminum chloride) is represented by M and dt is the time step. In a particular cell, the diffusion coefficient can be represented by the open pore diffusion coefficient (D_{op}), the product layer diffusion coefficient (D_{pl}) or an effective diffusion coefficient (D_{eff}) somewhere in between D_{op} and D_{pl} for when the product layer does not completely fill the cell during a particular time step. A diffusion resistance is used to determine D_{eff} through the partially filled cell as given by:

$$R_{eff} = R_{pl} + R_{op} = \frac{1}{D_{eff}} = \frac{\varepsilon_{pl}}{D_{pl}} + \frac{\varepsilon_{op}}{D_{op}} \qquad (7)$$

The volume fraction taken up by the produce layer and the open pore are given by ε_{pl} and $\varepsilon_{op,}$ respectively.

Figure 7 shows the experimental HCl uptake in kg, against the best fit model with the parameters given in Table 2. The model was calibrated using two parameters: the reaction rate at the, k_r, and the diffusion coefficient through the product layer, D_{pl}. Scanning electron microscopy (SEM) was used to estimate the average pore radius, as well as the porosity of the entire oxide layer. This porosity, given in Table 2, is a fixed value for the

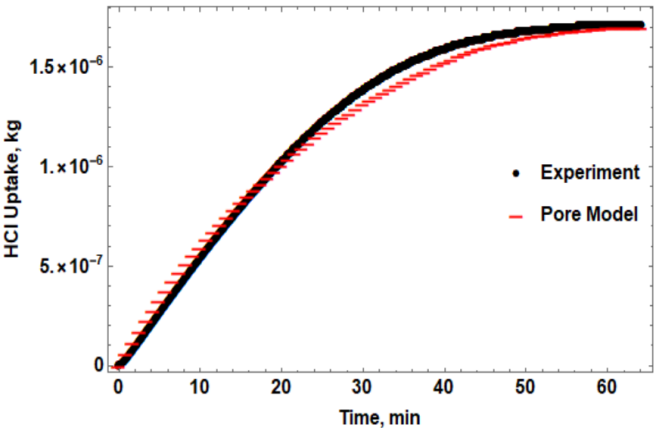

Figure 7: Uptake of HCl mass by anodized aluminum oxide layer.

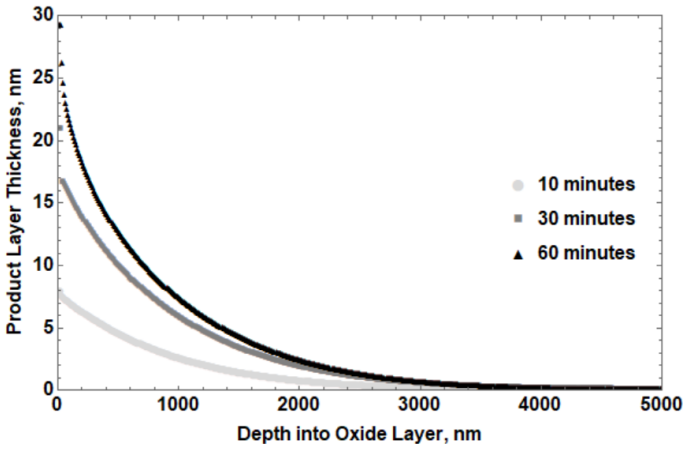

Figure 8: Product layer front as a function of depth into oxide layer.

Table 2: Parameters used in the pore model

Diffusion coefficient of product layer: D_{pl}	2.75×10^{-13} m^2/s
Diffusion coefficient of pore: D_{op}	1.85×10^{-9} m^2/s
Reaction rate at pore wall: k_r	5.00×10^{-5} m/s
Pore radius	30 nm
Porosity of oxide layer	0.15
HCl concentration at the inlet	43.1 ppm

sample and is not to be confused with the porosity of the single pore, which decreases as the aluminum chloride product layer forms. Additionally, pore radius and the porosity of the oxide layer were inferred from a combination of literature, and knowledge of the anodization voltage [19-22]. The porosity could then be used to determine the number of pores and distance between the pores as outlined in Figure 1B, representing the oxide-scale model This assumes that each pore being modeled and represented in the pore-scale in Figure 1C has the same diameter.

Figure 8 shows the product layer front at three different instances of time, with 30 nm being the maximum product layer thickness since that is the pore radius, and represents the pore closing up, thereby preventing further uptake of HCl. The 60-minute mark is when the product layer reaches 30 nm, and uptake slows drastically as shown in Figure 7.

The open pore diffusion coefficient of 1.85×10^{-9} m^2/s was used with the assumption that capillary condensation would be found in the pores. Studies using anodized nano channels and other nano channels have observed capillary condensation in pores between 10 and 60 nm [23,24]. Values for chlorine diffusion in water reported in the literature are consistent with this value [25].

The diffusion resistance described in Eq. (7) for individual cells can also be used to determine the increase in resistance from the pore, and assuming each pore is the same, the oxide layer in total. This could be used to develop an expression for the increased resistance in the reactor model. Further details of the model are discussed in [15].

RESULTS AND DISCUSSION

Qualitatively, the inferior fit between the experimental data and the reactor model with the anodized treatment vs. the stock and CCC can be seen by comparing Figures 5 and 6. The difference in standard error also gives quantitative data. The standard error between experiment and prediction is almost twice in the case of the anodized reactor model compared to the CCC and stock as given by Table 3.

Table 3: Standard error of models as compared to experiment.

Model Type	Standard Error Against Experiment (ppm)
Untreated	1.11
CCC	0.76
Anodized	3.08
Anodized with Eq. (8)	1.59
Anodized with Eq. (9)	1.62

It is possible that there are slight deviations in the chemical structure of the oxide layer, such as more silicon or magnesium, which would justify adjusting the calibration coefficients. During the calibration process, increasing A, generally brought the minimum concentration in the curve down, while increasing μ produced a faster recovery. However, changing the A and μ value drastically did little to change the prediction in the anodized case. For example, Figure 9A shows the reactor model with the stock sample using +/- 100% value of the baseline A value (A = 30,000) compared to Figure 9B with the anodized model. As expected, the minimum concentration in the stock prediction dropped noticeably as A was increased, while little to no change was noticed in the anodized prediction as A was varied. This is an indication that other physics are at work. It is known from the XPS results that chlorine is found much deeper in the oxide layer than in the stock or CCC samples. This means that the active sites are not all on the surface for the anodized

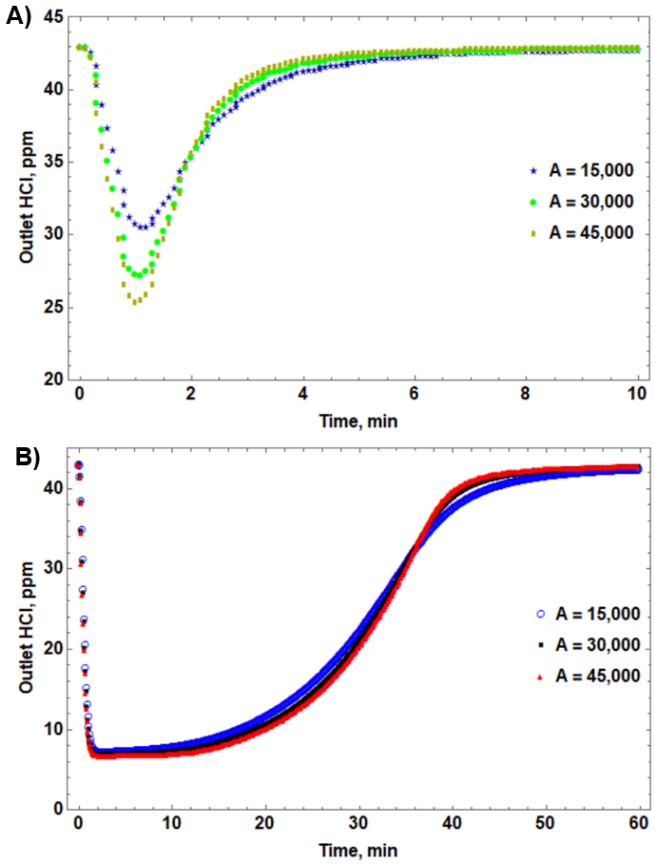

Figure 9: Stock (A) and anodized (B) reactor models with different calibration coefficients. *A was varied by +/- 100% to determine the sensitivity of each model.*

aluminum relative to the other aluminum, and that HCl needs to diffuse through the layer to get to an active site to react.

An expression for the increased diffusion resistance the buildup of aluminum chloride provides is given in Figure 10 along with the least square fit. In the pore model, the aluminum chloride layer builds until the diffusion resistance is too much

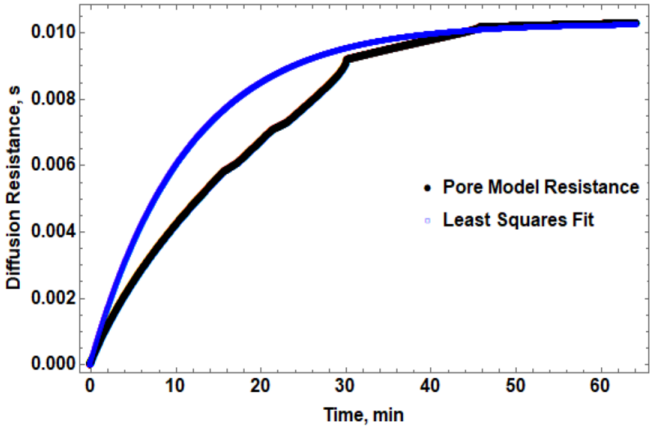

Figure 10: Diffusion resistance from pore model. *This resistance is used to determine the diffusion coefficient of the cells adjacent to the reacting surface.*

for further reaction to continue. This can be quantified in a diffusion resistance that can be used in the reactor model. Analogous to Eq. (7), the ratio of the area fraction taken up by the product layer or open pore and its respective diffusion coefficient is added in series to get an expression of the diffusion resistance. This resistance correlates proportionality to a decrease in the effective diffusion coefficient used in the adjacent cells to the reacting surface in the reactor model. The expression for this effective diffusion coefficient is shown in Figure 11 and given by the expression:

$$D_{eff} = 1.55x10^{-5}e^{-.0015t} \qquad (8)$$

Placing Eq. (8) as the effective diffusion coefficient near the reacting surface drastically decreased the standard error as seen in Table 3. This expression, however, would only hold in this particular reactor simulation with the same flow conditions and initial concentrations.

To expand the generality of this method, an expression that is not purely a function of time must be developed. The speed in which the sample saturates is dependent on the sum of HCl that makes it to the wall. Integrating the wall concentration with time and performing a least square fit to the original curve, Eq. (8), gave an expression for the decreased diffusion coefficient shown also in Figure 11 and given by:

$$D_{eff} = 1.55x10^{-5}e^{-18\sqrt{\int_{t_0}^{t} c_w}} \qquad (9)$$

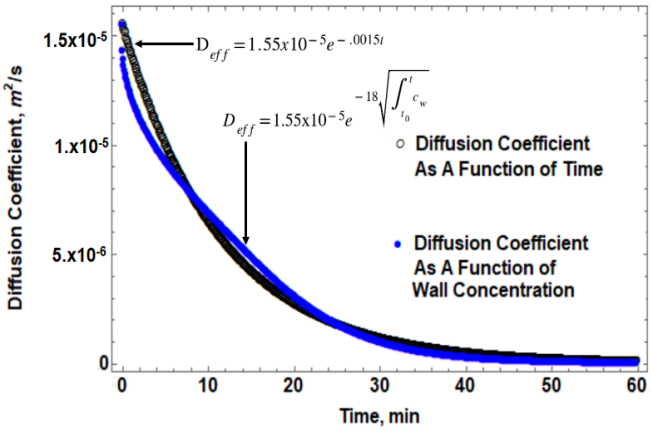

Figure 11: Diffusion coefficient of cells adjacent to the reacting surface. *Black line represents the diffusion coefficient purely as a function of time, Eq. (8), while the blue line is fitted to the black line to be a function of cell center concentration of cells adjacent to the reacting surface, Eq. (9).*

Using the expression in Eq. (9) in the reactor model gave a similar prediction as using Eq. 8, as expected, and can be seen in Figure 12.

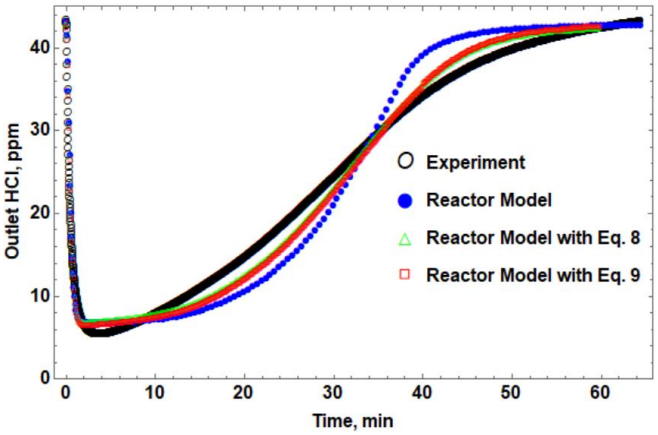

Figure 12: Outlet concentration in the reactor experiments and models. *Adjusting the diffusion coefficient in the reactor model brings up the concentration faster for a better prediction.*

The further development of the reactor model to incorporate pore-scale phenomenon will allow for more accurate predictions at reduced computational costs. This is essential as spacecraft fire simulations will be in the length scale of meters, while the physics that govern acid gas adsorption will be micro- and nano-scale in length. More accurate predictions of the uptake of acid gas in a fire scenario will help engineers design better smoke detectors, and post-fire cleanup practices. Knowing how much HCl remains in the atmosphere and how much remains in the surfaces will aid in the development of procedures for crew health and safety in terms of when it is optimal to return to a fire damaged section of the spacecraft.

CONCLUSION

Two models were utilized and eventually combined to predict the uptake of HCl onto anodized aluminum. A single-scale reactor model with a 1-step global reaction was able to predict uptake of treated aluminum with thin oxide layers better than with thick oxide layers. A multiscale model was developed to address aluminum samples with thick oxide layers. In this model information derived from a pore-scale model was integrated with the reactor-scale model. The pore-scale model was utilized to predict the uptake of HCl by the thick oxide layer of the anodized aluminum. In the pore-scale model, the saturation of the sample was due to the increased aluminum chloride layer build up at the pore walls which increased the diffusion resistance of the HCl to the pore wall, slowing the reaction to a stop. An expression of this increased diffusion resistance was used in the reactor model of the anodized aluminum to increase the prediction accuracy. This expression took the form of a decreased diffusion coefficient as a function of time in the cells adjacent to the reacting surface. The expression was then modified to be a function of integrated HCl wall concentration so that it could be used in other reactor models and spacecraft simulations.

ACKNOWLEDGEMENTS

This research was funded by the Saffire Project within NASA's Advanced Exploration Systems Division. The authors like would like to thank the project manager Gary Ruff and the principal investigator David Urban for their leadership on the project and Gordon Berger and Dan Gotti for their technical expertise and engineering design efforts.

REFERENCES

[1] Fujita, O., 2015, "Solid combustion research in microgravity as a basis of fire safety in space," *Proceedings of the Combustion Institute*, Vol. 35.3, pp. 2487-2502.

[2] Xiaoyang, Z., Liao, Y-T., T., Johnston, M.C., James, S., Ferkul, P., V., and Olson, S., L., 2017, "Concurrent flame growth, spread, and quenching over composite fabric samples in low speed purely forced flow in microgravity," *Proceedings of the Combustion Institute*, Vol. 36.2, pp. 2971-2978.

[3] Meyer, M. E., Mulholland, G. W., Bryg, V., Urban, D. L., Yuan, Z.-G., Ruff, G. A., Cleary, T., and Yang, J., 2015, "Smoke Characterization and Feasibility of the Moment Method for Spacecraft Fire Detection," *Aerosol Sci. Technol.*, Vol. 49.5, pp. 299–309.

[4] Ruff, G. A., Urban, D. L., Fernandez-Pello, A. C., T'ien, J. S., Torero, J. L., Legros, G., Eigenbrod, C., Smirnov, N., Fujita, O., Cowlard, A. J., Rouvreau, S., Minster, O., Toth, B., and Jomaas, G., 2014, "Spacecraft Fire Experiment (Saffire) Development Status," *Proceedings of the ICES2014*, July 13 – 17, 2014, Tucson, Arizona, Paper Number ICES-2014-265.

[5] Jomaas, G., Torero, J. T., Eigenbrod, C., Niehaus, J., Olson, S. L., Ferkul, P. V., Legros, G., Fernandez-Pello, C., Cowlard, A. J., Rouvreau, S., Smirnov, N., Fujita, O., T'ien, J. S., Ruff, G. A., and Urban, D. L., 2015, "Fire Safety in Space – Beyond Flammability Testing of Small Sample," *Acta Astronautica*, Vol. 109, pp. 208-216.

[6] Ruff, G. and Urban, D., 2016, "Operation and Development Status of the Spacecraft Fire Experiments (Saffire)," *Proceedings of the ICES2016*, July 10 – 14, Vienna, Austria, Paper Number ICES-2016-428, Texas Tech University Libraries.

[7] Ferkul, P. V., Olson, S., Urban, D. L., Ruff, G. A., Easton, J., T'ien, J. S., Liao, Y.-T. T., Fernandez-Pello, A. C., Torero, J. L., Eigenbrod, C., Legros, G., Smirnov, N., Fujita, O., Rouvreau, S., Toth, B., and Jomaas, G., 2017, "Results of Large-Scale Spacecraft Flammability Tests," *Proceedings of the ICES2017*, July 16 – 20, 2017, Charleston, South Carolina, Paper Number ICES-2017-224.

[8] Friedman, R., 1996, "Fire safety in spacecraft," *Fire and Materials*, Vol. 20.5, pp. 235-243.

[9] Beitel, J. J., Bertelo, C. A., Carroll Jr, W. F., Gardner, R. O., Grand, A. F., Hirschler, M. M., and Smith, G. F., 1986, "Hydrogen Chloride Transport and Decay in a Large

Apparatus I. Decomposition of Poly (Vinyl Chloride) Wire Insulation in a Plenum by Current Overload," *Journal of fire sciences*, Vol. 4.1, pp. 15-41.

[10] Galloway, F. M., and Hirschler, M. M., 1987, "Hydrogen chloride release from poly (vinyl chloride): model for its decay," *European polymer journal*, Vol. 23.9, pp. 667-676.

[11] Kumar, C. S., Mayanna, S. M., Mahendra, K. N., Sharma, A. K., and Rani, R. U., 1999, "Studies on white anodizing on aluminum alloy for space applications," *Applied Surface Science*, Vol. 151.3-4, pp. 280-286.

[12] Pugel, D. B., Rummel, J. R., and Conley, C., 2016, "Tiny houses: Planetary protection-focused *materials selection for spaceflight hardware surfaces," Proceedings of the IEEE Aerospace Conference*, March 5- 12, 2016, Big Sky, Montana, Paper Number AERO.2016.7500727.

[13] Niehaus, J. E., Gokoglu, S. A., Berger, G., Easton, J., and Mazumder, S., 2020, "Modeling hydrogen chloride and aluminum surface interactions for spacecraft fire safety applications," *Journal of Spacecraft and Rockets*, Vol. 57.2, pp. 217-224.

[14] Niehaus, J., Gokoglu, S., Mazumder, S., Berger, G., and Easton, J., 2020, "Effect of Humidity on Surface Interactions of Gaseous HCl and Aluminum for Spacecraft Fire Safety Applications," *Proceedings of the ICES2020*, July 12 – 16, 2020, Virtual Event, Paper Number ICES-2020-341.

[15] Niehaus, J., Gokoglu, S., Mazumder, S., Berger, G., and Easton, J., 2021, "Modeling the Uptake of Hydrogen Chloride onto Interior Spacecraft Materials," *Proceedings of the ICES2021*, July 12 – 15, 2021, Virtual Event, Paper Number ICES-2021-271.

[16] Paereli, S., 2015, "Sorption of hydrogen chloride on solid sorbents," *MS thesis*, Chemical Engineering Dept., Norwegian University of Science and Technology.

[17] O'Mara, M. M., 1977, "Combustion of PVC" *Pure and Applied Chemistry*, Vol. 49.5, pp. 649-660.

[18] Mazumder, S., 2015, "Numerical methods for partial differential equations: finite difference and finite volume methods," *Academic Press*.

[19] Chen, Z., and Lu, C., 2005, "Humidity sensors: a review of materials and mechanisms," *Sensor letters*, Vol. 3.4, pp, 274-295.

[20] Nahar, R. K., 2000, "Study of the performance degradation of thin film aluminum oxide sensor at high humidity," *Sensors and Actuators B: Chemical*, Vol. 63, pp. 49-54.

[21] Peng, D., Jensen, C. D., Juliano, T. J., Gregory, J. W., Crafton, J., Palluconi, S., and Liu, T., 2013. "Temperature-compensated fast pressure-sensitive paint," *AIAA journal*, Vol. 51.10, pp. 2420-2431.

[22] Jani, A., Losic, D., and Voelcker, N., 2013, "Nanoporous anodic aluminium oxide: Advances in surface engineering and emerging applications," *Progress in Materials Science*, Vol. 58.5, pp. 636-704.

[23] Casanova, F., Chiang, C. E., Li, C. P., Roshchin, I. V., Ruminski, A. M., Sailor, M. J., and Schuller, I. K., 2008, "Gas adsorption and capillary condensation in nanoporous alumina films," *Nanotechnology*, Vol. 19.31, pp. 315709-315714.

[24] Bruschi, L., Mistura, G., Liu, L., Lee, W., Gösele, U., and Coasne B., 2010, "Capillary condensation and evaporation in alumina nanopores with controlled modulations," *Langmuir*, Vol. 26.14, pp. 11894-11898.

[25] Leaist, D. G., 1986, "Absorption of chlorine into water," *Journal of solution chemistry*, Vol. 15.10, pp.827-838.